

PAPER

## Elastic wave propagation in the elastic metamaterials containing parallel multi-resonators

To cite this article: Yongjun Tian *et al* 2019 *J. Phys. D: Appl. Phys.* **52** 395301

View the [article online](#) for updates and enhancements.





**IOP | ebooks™**

Bringing you innovative digital publishing with leading voices to create your essential collection of books in STEM research.

Start exploring the collection - download the first chapter of every title for free.

# Elastic wave propagation in the elastic metamaterials containing parallel multi-resonators

Yongjun Tian<sup>1,2</sup>, Jiu Hui Wu<sup>1,4</sup>, Hongliang Li<sup>2</sup>, Cansong Gu<sup>2</sup>,  
Zhengrui Yang<sup>1,2</sup>, Ziting Zhao<sup>2</sup> and Kuan Lu<sup>3,4</sup>

<sup>1</sup> School of Mechanical Engineering and State Key Laboratory for Strength and Vibration of Mechanical Structures, Xi'an Jiaotong University, Xi'an 710049, People's Republic of China

<sup>2</sup> China Automotive Technology and Research Center Co., Ltd, Tianjin 300300, People's Republic of China

<sup>3</sup> School of Mechatronic Engineering, North University of China, Taiyuan 030051, People's Republic of China

E-mail: [ejhwu@mail.xjtu.edu.cn](mailto:ejhwu@mail.xjtu.edu.cn) and [elukuan@163.com](mailto:elukuan@163.com)

Received 25 March 2019, revised 12 June 2019

Accepted for publication 28 June 2019

Published 22 July 2019



CrossMark

## Abstract

This paper presents the modeling technique, design method, a new working mechanism and influence factors for elastic metamaterials (EMs) with parallel multi-resonators for broadband elastic vibration suppression. The general formula of the effective mass is deduced, and the effects of the relevant structural parameters on the frequency regions of the negative effective mass are illustrated in details. Subsequently, the dispersion relation and transmission spectrum of the EMs are studied. Based on the theoretical approach, the EMs plates were proposed, and the formation mechanism of the band gaps are analyzed by studying the displacement field of the eigenmodes at the band gaps edges. The related results well confirm that the novel EMs induces multi-frequency negative effective mass, and the number of the regions is equal to the number of the local resonators. The start frequencies of the band gaps are decided by the natural frequencies of each resonator, and the width of frequency band with negative effective mass can be broadened by enlarging the mass ratio of the local resonator. The EMs plate with the thickness of only 2.5 mm designed on the basis of theoretical research exhibits two flexural vibration band gaps (FVBGs) with the total width of 78.4 Hz below 200 Hz, which has been verified by the transmission testing experiments. For the formation mechanism of the FVBGs, the vibration is localized in the according resonator at the lower edge of each band gap, while at the upper edges the local resonance mass and the base plate vibrate in a reverse phase. Based on the theoretical and numerical analyses, the EMs with multiple parallel local resonators would be used in various fields, such as noise and vibration isolation, filters, and other renewed devices.

Keywords: elastic metamaterials, low-frequency vibration, multi-resonators

(Some figures may appear in colour only in the online journal)

<sup>4</sup> Author to whom any correspondence should be addressed.

## 1. Introduction

Elastic metamaterials (EMs), a novel kind of artificial periodic materials or structures, have received significant attention for their exceptional physical properties, such as negative effective mass and moduli, and negative refractive index [1–16]. The existence of the band gaps for EMs can prohibit vibration propagation in any direction, which can be used to design the low-frequency vibration isolators or frequency filters.

There are exactly three different formation mechanisms of the band gaps for EMs, namely Bragg scattering, local resonance, and hybridization. The Bragg scattering bandgap is caused by multiple scatterings of the periodic inclusions, the wavelength of the band gap frequencies is as the same order of the structural period [1, 2]. The second mechanism employs the resonant vibration of the local resonance mass working against the excitation of the incident elastic waves to attenuate the vibration [3–14]. The frequency range of the band gap based on this mechanism is almost two orders of magnitude lower than that of the Bragg scattering. The third kind of bandgap formation mechanism is attributed to the coupling effects of local resonances and Bragg scattering, which is why they have been called hybridization gaps [15, 16]. Also among the above EMs structures, the local resonance EMs have been widely researched and developed for their excellent low-frequency vibration/acoustic suppression characteristics. By placing the rubber-coated lead spheres in an epoxy matrix, the EMs with negative effective mass was firstly proposed by Liu *et al* [3], and the formation mechanism of the negative effective mass can be well explained by the simple mass-in-mass spring structures. Subsequently, the conception of the EMs was introduced in the design of vibration reduction in engineering components, such as bars, beams, and plates [17–35]. Previous works are mainly focused on the single negativity resonators of the EMs, and the negative effective mass only exhibits within a very narrow frequency region, which greatly limits its further development. For these reasons, the EMs with the multi-degree of freedom resonators are studied to deal with such problems. In fact, the EM with the two-degrees-of-freedom local resonator was firstly reported by Yu *et al* [36], the vertical and rotational vibrations of the local resonance mass were considered to obtain a wider low-frequency band gap. On the basis of his research, Lu *et al* redesigned the EM beam with two separated band gaps through the unequal distance between the two supporting springs to the center of mass of the local resonance mass [37]. Huang *et al* investigated a two-resonator mass-in-mass lattice system theoretically. He found that the major band gaps are determined mainly by the outermost mass, and the minor band gap can be achieved by changing the microstructure parameters [38]. Tan *et al* optimize the band gaps of the dual-resonator EM, and the advantage of elastic wave attenuation over a wider frequency region was demonstrated [39]. Hussein *et al* studied the dispersion relation of a viscous damped two-resonator metamaterial which exhibits higher dissipation throughout the spectrum, and because of the local resonance, a

damping emergence phenomena was illustrated [40]. The ideas of the multi-degree-of-freedom resonators are subsequently introduced in the design of vibration reduction for the beam and plate [41–49]. All the previously mentioned mass-spring models have the same structure, and there are some difficulties in manufacturing and processing of the EMs. In view of this, Pai and Xiao both reported the new EMs bars with many tiny spring-mass subsystems attached in parallel, the band gaps with the number being equal to the number of the resonators can be found, and the formation mechanism of the band gaps were explained theoretically [41–46]. However, the aforementioned analyses were mainly concerned with the specific EMs structures and less on the theoretical equivalent mass-spring system, which may limit the use of this type of EMs.

In this paper, the negative effective mass of the EMs with multiple parallel local resonators is investigated theoretically. The general formula of the effective mass is deduced, and the effects of the structural parameters on the frequency regions of the negative effective mass are illustrated in details. Subsequently, the dispersion relation and transmission spectrum of this type of EMs are studied, based on the theoretical approach. The EMs plates were proposed, and the formation mechanism of the band gaps is analyzed by studying the displacement field of the eigenmodes at the band gaps edges.

## 2. Lattice model of parallel multi-resonators

### 2.1. Negative effective mass

Consider an infinitely long one-dimensional lattice system consisting of parallel multi-resonators, as shown in figure 1. The outer masses  $m_0$  are connected periodically by the outer springs  $k_0$  with the spacing of  $L$ , and the local resonance mass  $m_i$  is linked to the outer mass  $m_0$  by the spring  $k_i$  in parallel. The unit cell of the lattice model, as shown in figure 1(b), is used to study the effective mass of the parallel multi-resonators EMs.

The motion equation of the unit cell can be given by

$$M\ddot{U} + KU = F, \quad (1)$$

with

$$M = \begin{bmatrix} m_0 & 0 & 0 & \cdots & 0 & 0 \\ 0 & m_1 & 0 & \cdots & 0 & 0 \\ 0 & 0 & m_2 & \ddots & 0 & 0 \\ \vdots & \vdots & \ddots & \ddots & \vdots & \vdots \\ 0 & 0 & 0 & \cdots & m_{n-1} & 0 \\ 0 & 0 & 0 & \cdots & 0 & m_n \end{bmatrix}, \quad (2)$$

$$K = \begin{bmatrix} k_1 + k_2 + \cdots + k_n & -k_1 & -k_2 & \cdots & -k_{n-1} & -k_n \\ -k_1 & k_1 & 0 & \cdots & 0 & 0 \\ -k_2 & 0 & k_2 & \ddots & 0 & 0 \\ \vdots & \vdots & \ddots & \ddots & \vdots & \vdots \\ -k_{n-1} & 0 & 0 & \cdots & k_{n-1} & 0 \\ -k_n & 0 & 0 & \cdots & 0 & k_n \end{bmatrix}, \quad (3)$$

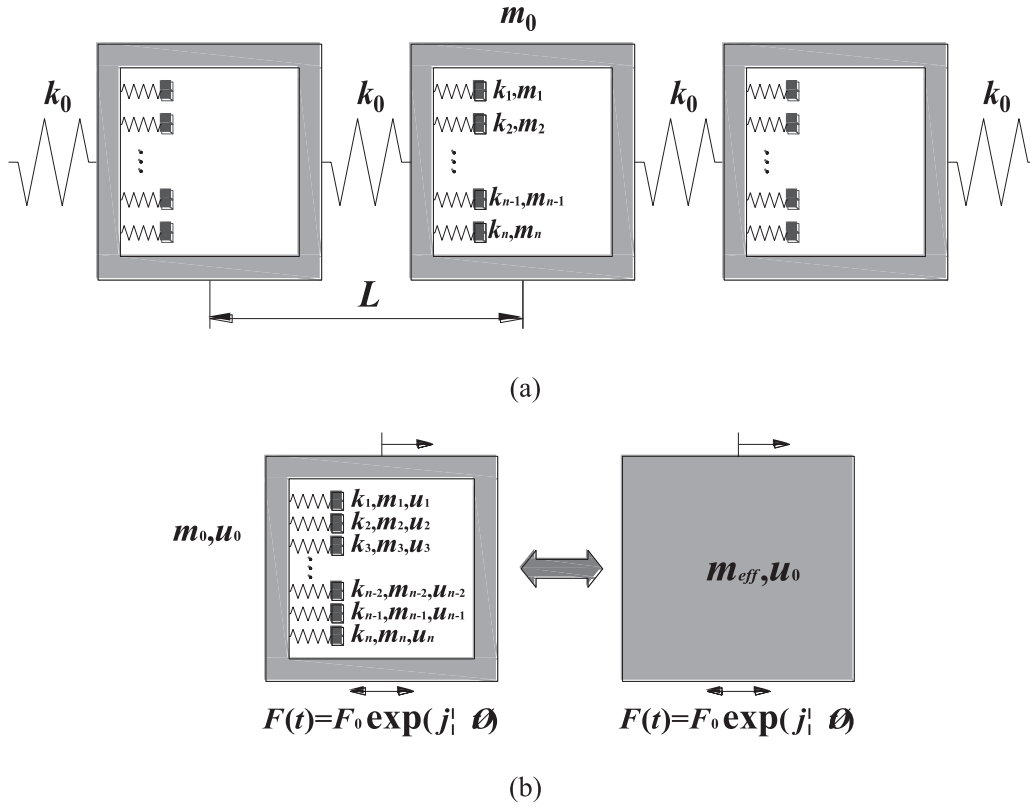


**Figure 1.** (a) The one-dimensional lattice system consisting of parallel multi-resonators, (b) the unit cell of the lattice system and its effective mass.

$$U = \begin{bmatrix} u_0 \\ u_1 \\ \vdots \\ u_n \end{bmatrix}, \quad (4)$$

$$F = \begin{bmatrix} F \\ 0 \\ \vdots \\ 0 \end{bmatrix}, \quad (5)$$

where  $u_i = U_i \exp(j\omega t)$  denotes the displacement of the  $i$ th lump mass,  $F = F_0 \exp(j\omega t)$  is external force applied on the unit cell.

By solving the above equations, we can simplify the relation as

$$\left( m_0 + \sum_{i=1}^n m_i \frac{\omega_i^2}{\omega_i^2 - \omega^2} \right) \omega^2 U_0 + F_0 = 0, \quad (6)$$

where  $\omega_i = \sqrt{\frac{k_i}{m_i}}$  is the natural frequency of the  $i$ th resonator.

Previous work [14, 38, 45, 48, 49] has proved that the effective mass of the unit cell must satisfied the follow equation

$$F_0 = -m_{eff}^{(n)} \omega^2 U_0. \quad (7)$$

According to equations (6) and (7), the effective mass of the EMs with  $n$  parallel multi-resonators can be expressed as

$$m_{eff}^{(n)} = m_0 + \sum_{i=1}^n m_i \frac{\omega_i^2}{\omega_i^2 - \omega^2}. \quad (8)$$

From equation (8) it can be found that, the effective mass of the composite system is closely related to the natural frequency of each resonator, and there will be  $n$  negative mass regions for the EMs with  $n$  resonators.

For a more intuitive indication, the effective mass of the lattice model with  $n$  ( $n = 1, 2, 3, 4$ ) resonators are illustrated in figure 2. In the calculation, the total mass of the local resonance mass is remained constant, and the relevant parameters of the distributed masses used are shown in detail, in table 1. Meanwhile, the equivalent stiffness of the springs is assumed to the same, i.e.  $k_1 = k_2 = k_3 = k_4 = 1 \text{ N m}^{-1}$ .

From figure 2, it can be found that the number of the frequency regions having negative masses increases from one to four with the number of the resonators increasing from one to four, and the number of the negative mass regions are equal to the number of the resonators. Table 2 lists the bandwidths as well as the start-stop frequencies of the negative effective mass regions. It is easy to see that the total bandwidth of the negative effective mass region is enlarged from  $0.5774 \text{ rad s}^{-1}$  for the single-resonator model to  $1.1316 \text{ rad s}^{-1}$  for the quad-resonator model.

Further manipulation of the equation (8), the effective mass of the meta-composite system can be re-represented as follows:

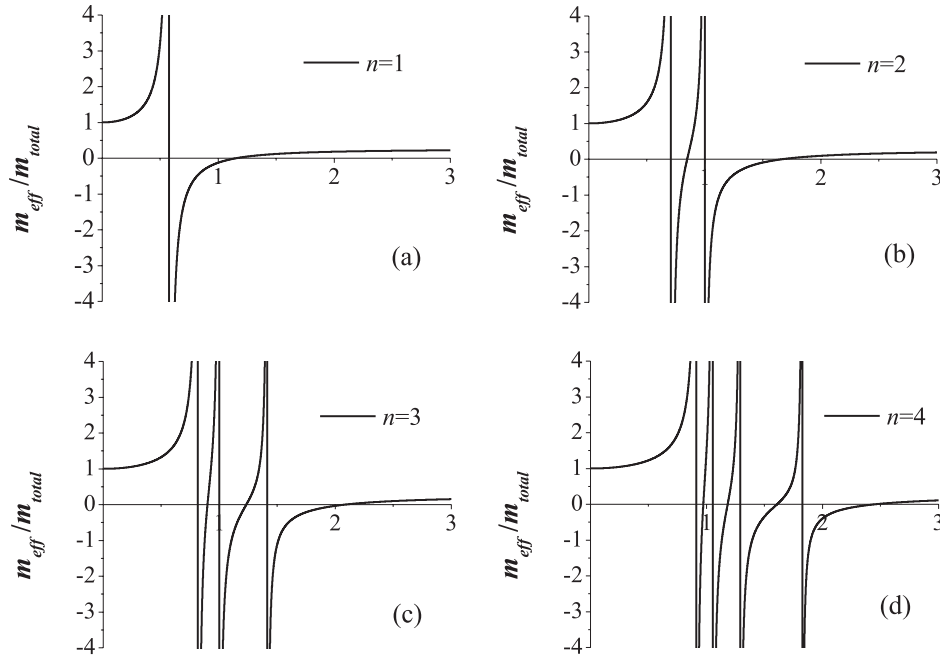


**Figure 2.** The normalized effective mass of the meta-composite system with (a) one single resonator, (b) two parallel resonators, (c) third parallel resonators, and (d) four parallel resonators.

**Table 1.** The relevant parameters used in the calculation.

$n$	$m_0$ (kg)	$m_1$ (kg)	$m_2$ (kg)	$m_3$ (kg)	$m_4$ (kg)
1	1.0	3.0	*	*	*
2	1.0	1.0	2.0	*	*
3	1.0	0.5	1.0	1.5	*
4	1.0	0.3	0.6	0.9	1.2

$$m_{eff}^{(n)} = m_0 + \left( 1 + \sum_{i=1}^n \alpha_i \frac{\omega_i^2}{\omega_i^2 - \omega^2} \right), \quad (9)$$

where  $\alpha_i = \frac{m_i}{m_0}$  is the ratio of the internal mass  $m_i$  to the outer mass  $m_0$ . From equation (9), it is obvious that the effective mass  $m_{eff}^{(n)}$  is dependent of two parameters, namely,  $\alpha_i$  and  $\omega_i$ , and their effects on band of the negative effective mass are shown in figures 3 and 4, respectively. In the investigation for the effects of  $\alpha_i$  on the negative effective mass, the natural frequencies of the resonators are set as follows:  $\omega_1 = 1 \text{ rad s}^{-1}$  for one single resonator;  $\omega_1 = 1 \text{ rad s}^{-1}$  and  $\omega_2 = 2 \text{ rad s}^{-1}$  for two parallel resonators, respectively;  $\omega_1 = 1 \text{ rad s}^{-1}$ ,  $\omega_2 = 2 \text{ rad s}^{-1}$ , and  $\omega_3 = 3 \text{ rad s}^{-1}$  for third parallel resonators, respectively; and  $\omega_1 = 1 \text{ rad s}^{-1}$ ,  $\omega_2 = 2 \text{ rad s}^{-1}$ ,  $\omega_3 = 3 \text{ rad s}^{-1}$ , and  $\omega_4 = 4 \text{ rad s}^{-1}$  for four parallel resonators, respectively. While for the investigation for the effects of  $\omega_i$  on the negative effective mass, the mass ratios  $\alpha_i$  are set as follows:  $\alpha_1 = 1$  for one single resonator;  $\alpha_1 = \alpha_2 = 1$  for two parallel resonators, respectively;  $\alpha_1 = \alpha_2 = \alpha_3 = 1$  for third parallel resonators, respectively; and  $\alpha_1 = \alpha_2 = \alpha_3 = \alpha_4 = 1$  for four parallel resonators, respectively.

As shown in figure 3, the cut-off frequency of each negative effective mass band gradually increases with the increasing

$\alpha_1$ , while the start frequency remains the same for the natural frequency of each local resonator keeping constant, which greatly broadens the regions of the negative effective mass. As shown in figure 4, it can be found that both the start frequency and the cut-off frequency of each negative effective mass band increase linearly with the increase of  $\omega_i$ , but the increasing rate of the cut-off frequency is greater than that of the start frequency, which broadens the regions of the negative effective mass slightly. From the previously described analysis we can know that the start frequency of the meta-composite system depends on the natural frequency of each independent resonator, that is to say, the resonators are independent of each other in working and no coupling occurred among them, which is different from the multi-resonators in the previous works [41–49].

By comparing figures 3 and 4, it can also be found that the band gap width is more sensitive to parameter  $\alpha_i$  rather than  $\omega_i$ . This phenomenon can be explained as: when the resonance frequencies of the resonators keep constant, increasing the mass ratio  $\alpha_i$  also means increasing the equivalent spring stiffness  $k_i$ , which greatly enhance the interactions between the local resonators and the vibrations of the base matrix, and the bandwidth of the negative effective mass is therefore broadened; however, the increase of  $\omega_i$  only means the increase of equivalent spring stiffness  $k_i$ , and the interactions strength between the resonators and the base matrix is less than the former case, thus the broadening of band gap is not obvious.

## 2.2. Wave propagation characteristics

For the wave transmission in the EMs, an infinitely long one-dimensional (1D) lattice meta-composite system is considered as shown in figure 5.

**Table 2.** Frequency regions with negative effective mass.

MDOF model	Number of bands with negative effective mass	Frequency region (rad s <sup>-1</sup> )	Band width (rad s <sup>-1</sup> )	Total band-width (rad s <sup>-1</sup> )
Single-resonator	1	[0.5774,1.1548]	0.5774	0.5774
Dual-resonator	2	[0.7072,0.8480] [1.0000,1.6675]	0.1408 0.6675	0.8083
Tri-resonator	3	[0.8165,0.8990] [1.0000,1.2333] [1.4143,2.0825]	0.0825 0.2333 0.6682	0.9840
Quad-resonator	4	[0.9129,0.9726] [1.0541,1.1826] [1.2910,1.6079] [1.8258,2.4523]	0.0597 0.1285 0.3169 0.6265	1.1316

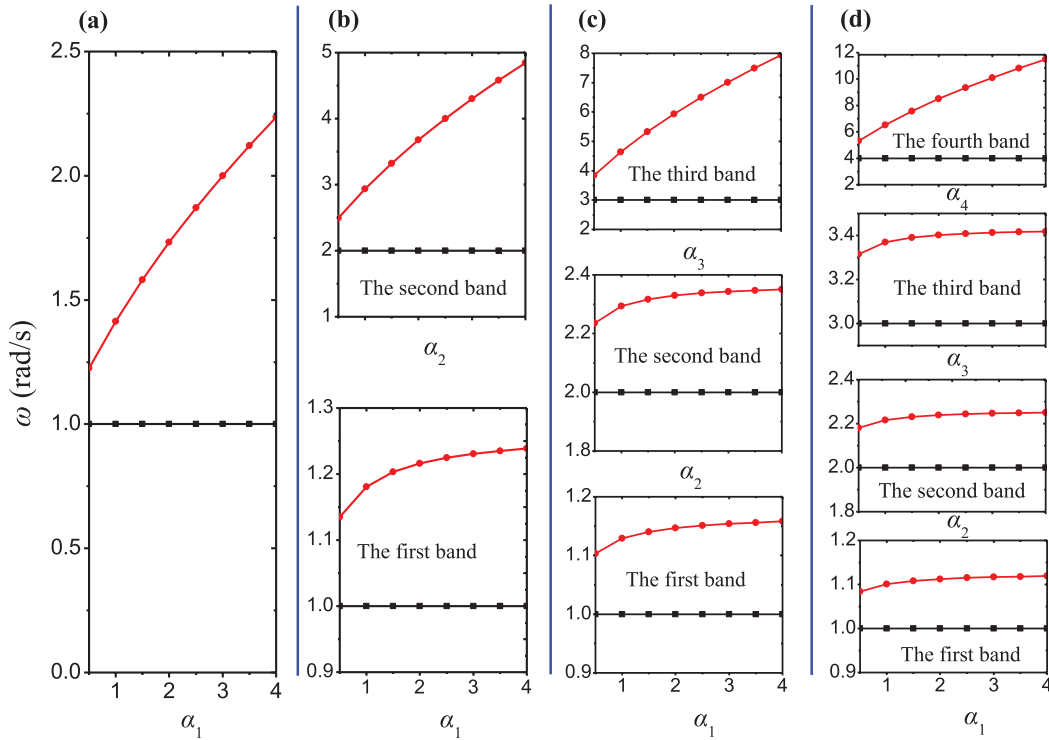


**Figure 3.** The effects of the parameter  $\alpha_i$  on the band of the negative effective mass.

For the harmonic wave propagation in the 1D lattice meta-composite system, the equations of motion for the  $j$ th unit cell can be expressed as

$$\begin{cases}
 m_0 \frac{d^2 u_0^{(j)}}{dt^2} + k_0 (2u_0^{(j)} - u_0^{(j-1)} - u_0^{(j+1)}) + k_1 (u_0^{(j)} - u_1^{(j)}) + \dots \\
 + k_{n-1} (u_0^{(j)} - u_{n-1}^{(j)}) + k_n (u_0^{(j)} - u_n^{(j)}) = 0 \\
 m_1 \frac{d^2 u_1^{(j)}}{dt^2} + k_1 (u_1^{(j)} - u_0^{(j)}) = 0 \\
 \vdots \\
 m_{n-1} \frac{d^2 u_{n-1}^{(j)}}{dt^2} + k_{n-1} (u_{n-1}^{(j)} - u_0^{(j)}) = 0 \\
 m_n \frac{d^2 u_n^{(j)}}{dt^2} + k_n (u_n^{(j)} - u_0^{(j)}) = 0
 \end{cases} \quad (10)$$

where  $u_\gamma^{(j)}$  represents the displacement of the mass ' $\gamma$ ' in the  $j$ th cell.

The harmonic wave solution for the  $j$ th element can be expressed as

$$u_\gamma^{(j)} = U_\gamma e^{i(qx - \omega t)}, \quad (11)$$

where  $U_\gamma$  is the complex wave amplitude,  $q$  is the wave number, and  $\omega$  is the angular frequency. Similarly, the harmonic wave solution for the  $(j + n)$ th unit cell can be then expressed as

$$u_\gamma^{(j)} = U_\gamma e^{i(qx + qnL - \omega t)}. \quad (12)$$

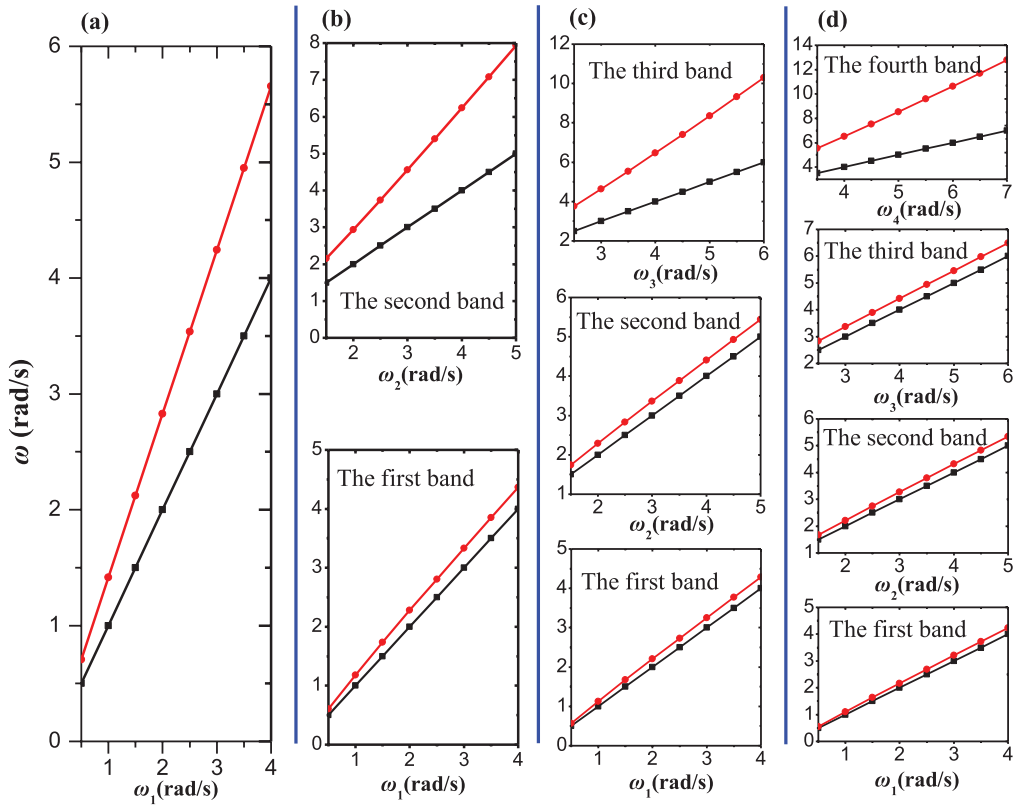


Figure 4. The effects of the parameter  $\omega_i$  on the band of the negative effective mass.

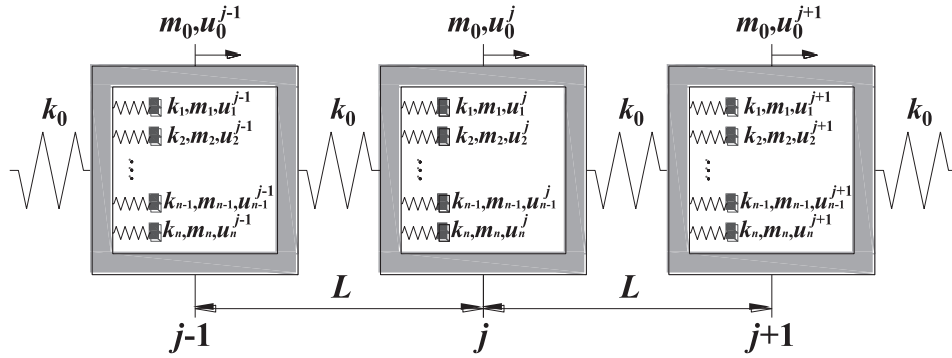


Figure 5. Wave propagation model of the 1D lattice meta-composite system.

By substituting the equations (11) and (12) into (10), we can get the control equation of the meta-composite system as

$$\begin{cases} -m_0\omega^2 U_0 + 2k_0 U_0 (1 - \cos qL) + k_1 (U_0 - U_1) + \dots + k_{n-1} (U_0 - U_{n-1}) + k_n (U_0 - U_n) = 0 \\ -m_1\omega^2 U_1 + k_1 (U_1 - U_0) = 0 \\ \vdots \\ -m_{n-1}\omega^2 U_{n-1} + k_{n-1} (U_{n-1} - U_0) = 0 \\ -m_n\omega^2 U_n + k_n (U_n - U_0) = 0 \end{cases} \quad (13)$$

The dispersion equation can be obtained as

$$m_0\omega^2 - 2k_0 (1 - \cos qL) + \sum_{i=1}^n m_i\omega^2 \frac{\omega_i^2}{\omega_i^2 - \omega^2} = 0. \quad (14)$$

Considering equation (8), the (14) can be rewritten as

$$m_{eff}^{(n)}\omega^2 - 2k_0 (1 - \cos qL) = 0. \quad (15)$$

The dispersion relations of the meta-composite system with one to four resonators are calculated, and the corresponding results are shown in figure 6. The relevant parameters used in the calculation are the same as those used in the investigation for the effective mass shown in figure 2.

As shown in figure 6, there are two, three, four, and five band branches for the meta-composite system with one single resonator, two parallel resonators, three parallel resonators, and four parallel resonators, respectively. The number of the band gaps is equal to that of the frequency regions of the negative mass, and their locations between them corresponds to each other very well by combining figures 2 and 6. This means that the negative effective mass of the meta-composite system has a significant attenuation in wave amplitude.

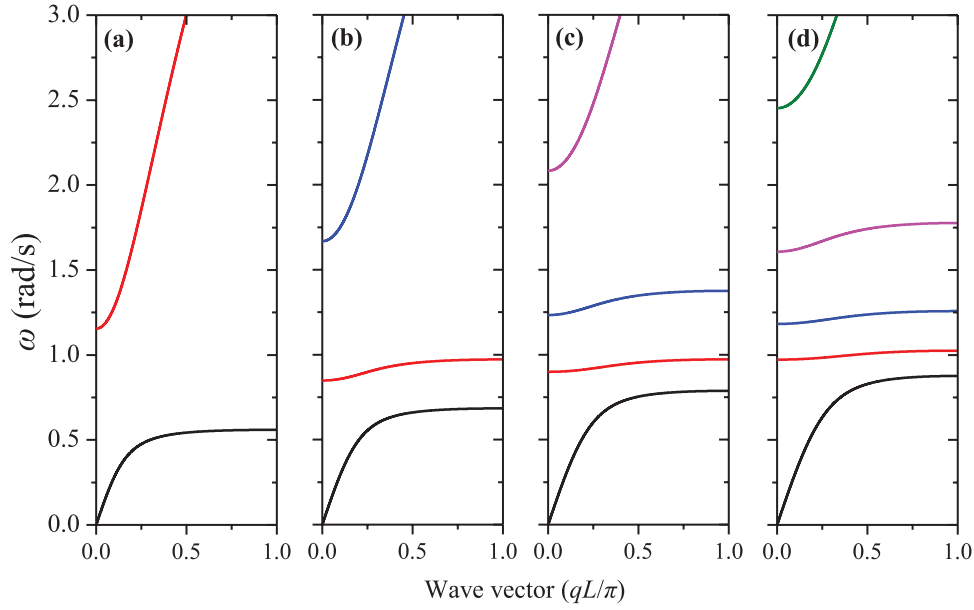


**Figure 6.** Dispersion relation curve of the meta-composite system with (a) one single resonator, (b) two parallel resonators, (c) three parallel resonators, and (d) four parallel resonators.

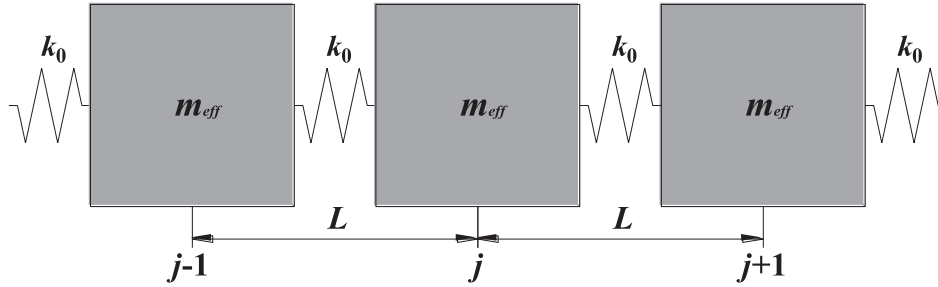


**Figure 7.**  $n$ -period one-dimension lattice meta-composite system with effective mass.

In the calculation of the transmission spectrum of the meta-composite system, the one-dimension complex system can be simplified as a mass-spring system with the effective mass shown in figure 7. The equivalent effective masses are also connected by the equal springs with stiffness  $k_0$ .

According to the structure shown in the figure 7, the motion equation of the  $n$ -period simplified system can be expressed as

$$(2k_0 - m_{eff}\omega^2) U_j - k_0(U_{j-1} + U_{j+1}) = 0, \quad j = 1, 2, \dots, n - 1 \quad (16)$$

$$(k_0 - m_{eff}\omega^2) U_n - k_0 U_{n-1} = 0, \quad (17)$$

where  $U_j$  represents the amplitude of the displacement for the  $j$ th equivalent unit cell.

Combining equations (16) and (17), we can obtain that

$$T_j = \frac{k_0}{k_0(2 - T_{j+1}) - m_{eff}\omega^2}, \quad j = 1, 2, \dots, n - 1 \quad (18)$$

$$T_n = \frac{k_0}{k_0 - m_{eff}\omega^2}, \quad (19)$$

where  $T_n = U_n/U_{j-1}$ . Thus the transmission spectrum of the 1D lattice system can be obtained as

$$TR = 20 \lg (|U_n/U_0|) = 20 \lg \left( \left| \prod_{j=1}^n T_j \right| \right). \quad (20)$$

Figures 8(a)–(d) show the transmission spectrum of the lattice system with six periods for the meta-composite structure with one to four resonators, respectively. The relevant parameters used in the calculation are the same as those in the investigation for the band structures described in figure 6. The obvious attenuation regions can be found in the transmission spectrum and their locations as well as the bandwidth are very close to those of the dispersion relation curves calculated above.

Through above analysis, we can see that this novel EMs is actually a multi-degree-of-freedom system, which is formed by arranging the single-degree-of-freedom resonator with different resonance frequency in parallel. Each resonator can open the bandgap independently, which is the most obvious feature of the EMs presented in this work. The desired locations of each bandgap can be adjusted more conveniently by adjusting the resonance frequency of the corresponding resonator. Moreover, compared with the traditional EMs in our pervious works, the interactions between the base plate and



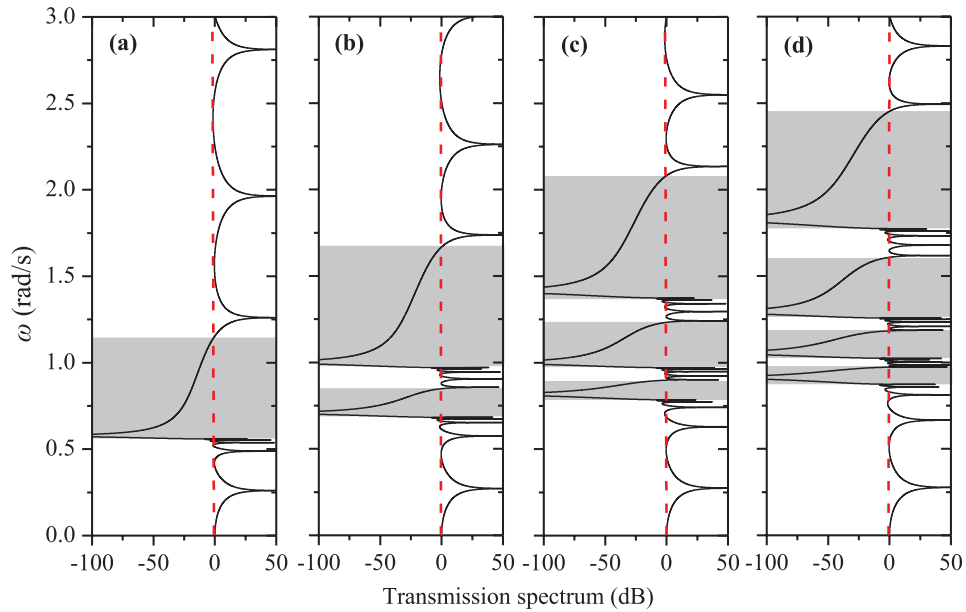


**Figure 8.** Transmission spectrum of the six-periods lattice system with (a) one single resonator, (b) two parallel resonators, (c) three parallel resonators, and (d) four parallel resonators.

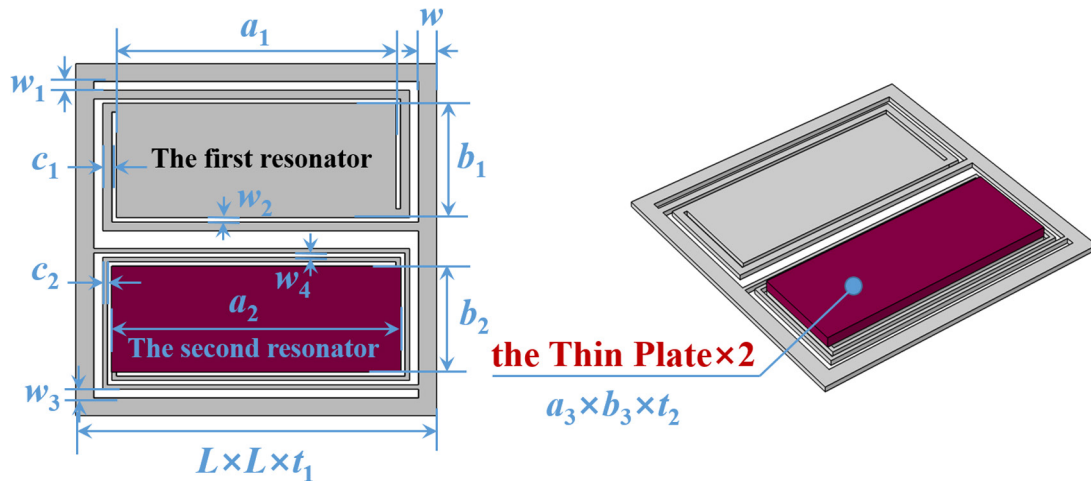


**Figure 9.** The continuum model of the elastic metamaterial plates with two resonators.

the resonance system are enhanced by the parallel arrangement of resonators, not by increasing the mass ratio, so that the vibration band gap can be broadened without increasing the overall resonance mass. In summary, the proposed EMs in this paper shows great advantages in the bandwidth and the adjustment of the locations of the band gaps, which would further enrich the forms of EMs and the formation mechanisms of band gaps.

### 3. Continuum model

#### 3.1. Model

The EMs plate, mimicking the lattice systems with two resonators, is proposed, and the unit cell is shown in figure 9. In the model, the size of the base plate is  $L \times L \times t_1$ , and the basic shapes of the two resonators are carved directly on the base plate, and two additional plates with size  $a_3 \times b_3 \times t_2$  are

attached on the second resonator for obtaining low-frequency vibration. The material of this EMs plate is all steel (Young’s modulus:  $2.1 \times 10^{11}$  Pa, mass density:  $7780 \text{ kg m}^{-3}$ , and Poisson’s ratio: 0.3), and its full size is as follows:  $L = 40 \text{ mm}$ ,  $t = 0.5 \text{ mm}$ ,  $w = 2 \text{ mm}$ ,  $a_1 = 31 \text{ mm}$ ,  $b_1 = 13 \text{ mm}$ ,  $c_1 = 1 \text{ mm}$ ,  $w_1 = 1 \text{ mm}$ ,  $w_2 = 0.5 \text{ mm}$ ,  $a_2 = 32 \text{ mm}$ ,  $b_2 = 12 \text{ mm}$ ,  $c_2 = 0.5 \text{ mm}$ ,  $w_3 = 0.5 \text{ mm}$ ,  $w_4 = 0.5 \text{ mm}$ ,  $a_3 = 32 \text{ mm}$ ,  $b_3 = 12 \text{ mm}$ , and  $t_2 = 1 \text{ mm}$ . As can be seen from the figure 9, this EMs plate adopts hollow design for two main purposes: one is that the hollow-out design does not introduce excessive thickness and mass compared with the traditional structures of our previous works [21, 25, 29, 49] (the overall thickness of the EMs plate is only 2.5 mm, and the extra weight added is also very small compared with other types of EMs plates), which is conducive to the realization of lightweight structure; the other is that the rubber (i.e. the springs in the lattice system model) in the traditional metamaterials is replaced by the matrix material (usually metal), which would alleviate the

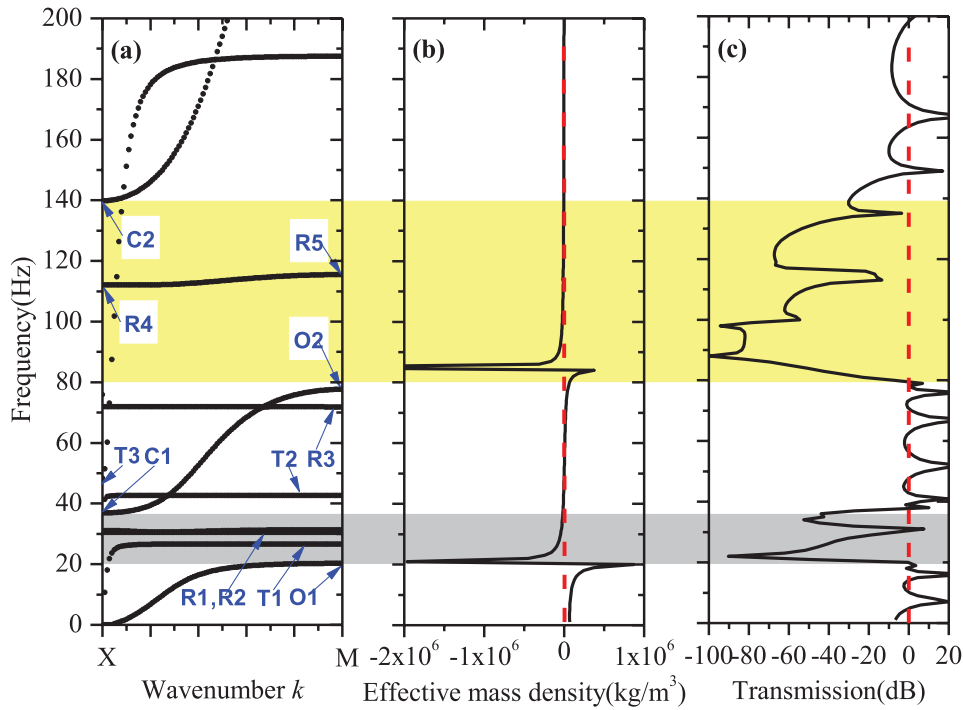


**Figure 10.** The calculation results for (a) band structures, (b) effective mass density, and (c) transmission spectrum of flexural vibration of the elastic metamaterial plate.

aging problem of rubber to some extent, and the service life of the EMs plate is improved.

### 3.2. Method

As the flexural wave is more prone to interact with air media, thus the out-of-plane vibration has been focused on in the investigation. In order to study the vibration characteristics of the EMs plates, the dispersion relations of the zero-order anti-symmetric Lamb wave (AO) mode are calculated by using the finite element method (FEM) which has been proved to be an efficient method in previous works [16, 21, 22, 25–29, 31, 32, 49]. The unit cell with periodic boundary conditions applied on the interfaces according to the Bloch–Floquet theory is considered, and by varying the value of the Bloch wave vector  $k$  in the irreducible first Brillouin zone, the band structures and the eigenmodes can be obtained. The transmission spectrum through the EMs plates with six unit cells is calculated. The harmonic displacement excitation is applied on the left side of the plate, while the average displacement response is picked up on the opposite side, then the transmission spectrum of the EMs plate can be obtained by equation (20). For the computational details can be referred to [16, 18, 39]. The calculation results of the band structures and the transmission spectrum for the EMs plates are shown in figure 10.

### 3.3. Band structures of the EMs plate

For the band structure shown in figure 10(a), it can be seen that seven bands exist in the frequency range from 0 Hz to 200 Hz, where two flexural vibration band gaps (FVBGs, the gray region and the yellow region) are involved. The lowest

FVBG is from 20.2 Hz to 37.8 Hz with a width of 17.6 Hz, which is between the first and fifth band. The second FVBG is from 78.6 Hz to 139.4 Hz with a width of 60.8 Hz, which is between the eighth and tenth band. The total width of the band gaps is 78.4 Hz. The effective mass density and the transmission spectrum of the EMs plate are also shown in figure 10(b) and (c), the detailed calculation method can be referred to the [27]. It can be found that there two frequency regions of negative effective mass density and obviously vibration attenuation can be found, and their locations both correspond well with the band gaps in figure 10(a).

### 3.4. Formation mechanism of the FVBGs

In order to further reveal the formation mechanism of the FVBGs, the eigenmode shapes and displacement vector fields of the modes labelled in figure 10(a) are shown in figure 11. The color map of figure 11 demonstrated the magnitude of the displacement vector fields which are calculated by  $\sqrt{u_x^2 + u_y^2 + u_z^2}$ . As mentioned in the previous works [1, 12, 19], when the frequency of incident elastic waves is closed to one of the nature frequency of the local resonator, the corresponding local resonance will be activated, and the two masses (the local resonance mass and the base mass) moved in reversed phase with a reaction force on the base mass against the elastic wave excitation. For the modes O1, O2, the start of the band gaps have the same form of vibration. When the incident frequency of the flexural wave is equal to the lower natural frequency of the first resonator, which activates the corresponding local resonance vibration (mode O1), and the reaction force provided by the local resonator would suppress the vibration of the base plate, thus the flexural wave cannot spread, which

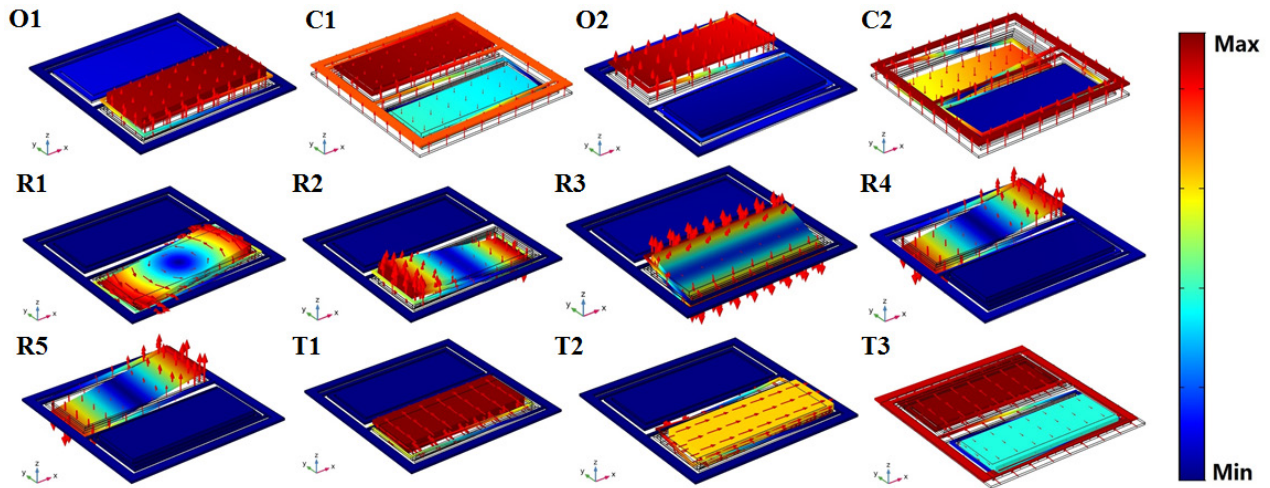


Figure 11. Eigenmode shapes and displacement vector field of the modes labelled in figure 10.

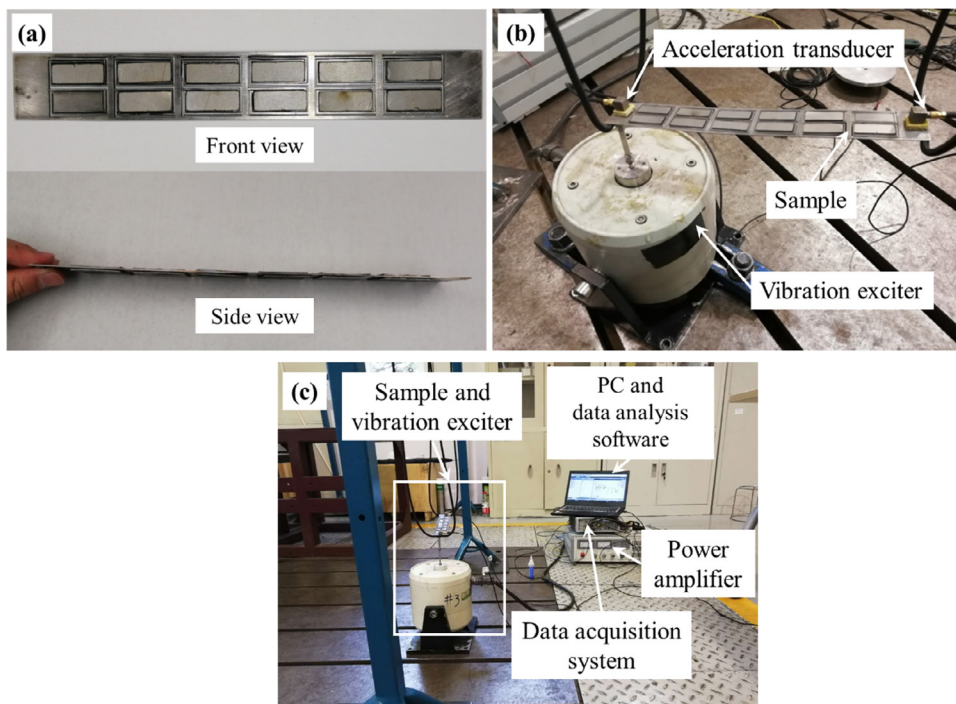


Figure 12. The test sample and the experimental measurement setup. (a) The test sample; (b) setup of the sample and the vibration exciter; and (c) the whole experimental setup.

opens the band gaps at this frequency. This is also true for mode O3. While for the cut-off of the band gaps, a dynamic balance occurred between the local resonance mass and the base plate, such the modes C1, and C2. The elastic wave can spread freely in these modes of vibration, and the band gaps closed at these frequencies. For modes R1, T1, T2, and T3, the vibrations of the local resonance mass are mainly concentrated in the  $x$ - $y$  plane, which are coupled with symmetric Lamb mode and shear-horizontal waves of the base plate, respectively. While for mode R2, R3, R4 and R5, the local resonance mass rotates along the center of the local resonance mass in  $x$ - or  $y$ -axis with the base plate keeping still. Compared with the excitation from the flexural wave mode, the resonances-induced out-of-plane force components applied on the plate are very small. Thus there exists no FVBG around this band.

Through the above analyses of theory and continuum models, we can see that the local resonators work independently of each other to open the band gaps and vibrate coupled to close the band gaps, which is the most obvious feature of the EMs proposed in this paper.

### 3.5. Experimental verification

To further verify the low-frequency FVBGs of the proposed structure, the transmission-measuring experiments of a EMs plate with six periodic local resonators is conducted. The boundary conditions in the  $y$ -direction do not make a significant impact on the transmission properties which have been verified in the previous work [26], so the EMs plate sample with only one layer in  $y$ -direction is considered in the experiment

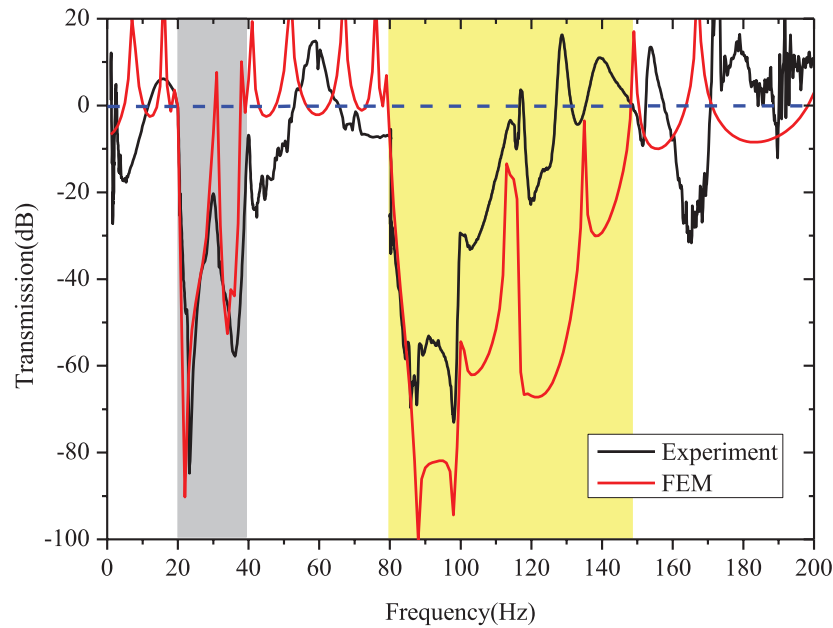


**Figure 13.** The experimental results for the transmission spectrum of the sample: experimental results (the black solid line), and FEM results (the red solid line).

(as shown in figure 12(a)). The corresponding EMs plate is made by 3D printing for realizing the desired high dimensional accuracy. The LMS test system with a vibration exciter (MB MODAL 2), a power amplifier, and two acceleration transducers (Dytran 3145AG) is employed in this experiment. A harmonic force is applied perpendicularly on the one side of the EMs plate, and two acceleration transducers are placed on the two opposite sides of the plate in  $x$ -direction, as shown in figure 12(b). A white-noise signal with bandwidth from 0 to 200 Hz is amplified to drive the vibration exciter, which transmits vibrations to the left side of the PC plate, and the signal of the acceleration of the flexural waves on the other side can be measured by the transducer. The photo of the whole experimental setup can be found in figure 12(c).

The transmission spectrum can be obtained by the LMS test. LAB software and shown as the blue solid curve in figure 13. It can be seen that there are two obvious attenuation regions in the experimental results (the black solid curve) whose locations are in good agreement with those of the FEM calculation results (the red solid curve). One can also see that the peak values of the experiment results are lower than those of the FEM results, for the reason that the effect of the material damping in the EMs plate is consider in the FEM calculation, and similar results can also been found in previous studies [17, 24, 26].

In summary, the relevant experimental results are able to fully prove that the broad FVBGs in the low-frequency range can be obtained in the proposed EMs plate with parallel multi-resonators in this research, which would provide a new way to deal with the challenging problems of the low-frequency vibration blow 200 Hz.

#### 4. Conclusion

In this paper, the negative effective mass of the EMs with multiple parallel local resonators is investigated theoretically.

The general formula of the effective mass is deduced, and the effects of the structural parameters on the frequency regions of the negative effective mass are illustrated in details. Subsequently, the dispersion relation and transmission spectrum of this type of EMs are studied. Finally, the EMs plates were proposed based on the above analyses, and the formation mechanisms of the band gaps are analyzed by studying the displacement field of the eigenmodes at the band gaps edges. Through the above analyses, we can draw the following conclusion:

- (1) The EMs with parallel multi-resonators induces multi-frequency negative effective mass, and the number of the regions is equal to the number of the local resonators. The start frequencies of the band gaps are decided by the natural frequencies of each resonator, and the width of frequency band for negative effective mass can be broadened by enlarging the mass ratio of the local resonator. Meanwhile, the multiple band gaps can be found with the locations corresponding to regions of negative effective mass, and the obvious vibration attenuation can be obtained within the stopping band.
- (2) For the EMs plates, the flexural wave band gaps with the number being equal to the number of the resonators can be found, and the locations of the calculated transmission spectrum are in good agreement with the corresponding frequency regions of the band gaps. At the lower edge of each band gap, the vibration is localized in the according resonator, while at the upper edges the local resonance mass and the base plate vibrate in a reverse phase or the base plate vibrates with large amplitude with the local resonance mass keeping still.
- (3) The sample of the EMs plates with two local resonators are made, and the transmission-measuring experiments of the sample with six periodic local resonators is conducted. By comparing the FEM results and experimental

measurements, the proposed EMs plate is demonstrated to possess the broad FVBGs in low-frequency range below 200 Hz, and the numerical calculation results are in good agreement with those of the experimental measurement, except for some differences due to the material damping of the EMs plate.

Based on the theoretical and numerical analyses, the EMs with multiple parallel local resonators would be used in various field, such as noise and vibration isolation, filters and other renewed devices.

## Acknowledgments

This work was supported by the National Natural Science Foundation of China (NSFC) under Grant No. 51675401, and the High-level Talents Scientific Research of North University of China in 2018 under Grant No. 304/11012305.

## ORCID iDs

Yongjun Tian  <https://orcid.org/0000-0002-1450-4109>

Kuan Lu  <https://orcid.org/0000-0001-5992-5540>

## References

- [1] Kushwaha M S, Halevi P, Dobrzynski L and Djafari-Rouhani B 1993 Acoustic band structure of periodic elastic composites *Phys. Rev. Lett.* **71** 2022
- [2] Martínez-Sala R, Sancho J, Sánchez J V, Gómez V, Llinares J and Meseguer F 1995 Sound attenuation by sculpture *Nature* **378** 241
- [3] Liu Z, Zhang X, Mao Y, Zhu Y Y, Yang Z, Chan C T and Sheng P 2000 Locally resonant sonic materials *Science* **289** 1734–6
- [4] Liu Z, Chan C T and Sheng P 2002 Three-component elastic wave band-gap material *Phys. Rev. B* **65** 165116
- [5] Li J and Chan C T 2004 Double-negative acoustic metamaterial *Phys. Rev. E* **70** 055602
- [6] Wang G, Yu D, Wen J, Liu Y and Wen X 2004 One-dimensional phononic crystals with locally resonant structures *Phys. Lett. A* **327** 512–21
- [7] Wang G, Wen X, Wen J, Shao L and Liu Y 2004 Two-dimensional locally resonant phononic crystals with binary structures *Phys. Rev. Lett.* **93** 154302
- [8] Fang N, Xi D, Xu J, Ambati M, Srituravanich W, Sun C and Zhang X 2006 Ultrasonic metamaterials with negative modulus *Nat. Mater.* **5** 452
- [9] Ding Y, Liu Z, Qiu C and Shi J 2007 Metamaterial with simultaneously negative bulk modulus and mass density *Phys. Rev. Lett.* **99** 093904
- [10] Huang H H, Sun C T and Huang G L 2009 On the negative effective mass density in acoustic metamaterials *Int. J. Eng. Sci.* **47** 610–7
- [11] Lee S H, Park C M, Seo Y M, Wang Z G and Kim C K 2010 Composite acoustic medium with simultaneously negative density and modulus *Phys. Rev. Lett.* **104** 054301
- [12] Liu X N, Hu G K, Huang G L and Sun C T 2011 An elastic metamaterial with simultaneously negative mass density and bulk modulus *Appl. Phys. Lett.* **98** 251907
- [13] Achaoui Y, Khelif A, Benchabane S, Robert L and Laude V 2011 Experimental observation of locally-resonant and Bragg band gaps for surface guided waves in a phononic crystal of pillars *Phys. Rev. B* **83** 104201
- [14] Liu Y, Su X and Sun C T 2015 Broadband elastic metamaterial with single negativity by mimicking lattice systems *J. Mech. Phys. Solids* **74** 158–74
- [15] Croëne C, Lee E J S, Hu H and Page J H 2011 Band gaps in phononic crystals: generation mechanisms and interaction effects *AIP Adv.* **1** 041401
- [16] Chen Y and Wang L 2014 Periodic co-continuous acoustic metamaterials with overlapping locally resonant and Bragg band gaps *Appl. Phys. Lett.* **105** 191907
- [17] Wen J, Wang G, Yu D, Zhao H and Liu Y 2005 Theoretical and experimental investigation of flexural wave propagation in straight beams with periodic structures: application to a vibration isolation structure *J. Appl. Phys.* **97** 114907
- [18] Wang G, Wen X, Wen J and Liu Y 2006 Quasi-one-dimensional periodic structure with locally resonant band gap *J. Appl. Mech.* **73** 167–70
- [19] Milton G W and Willis J R 2007 On modifications of Newton's second law and linear continuum elastodynamics *Proc. R. Soc. A* **463** 855–80
- [20] Huang H H and Sun C T 2009 Wave attenuation mechanism in an acoustic metamaterial with negative effective mass density *New J. Phys.* **11** 013003
- [21] Oudich M, Li Y, Assouar B M and Hou Z 2010 A sonic band gap based on the locally resonant phononic plates with stubs *New J. Phys.* **12** 083049
- [22] Hsu J C 2011 Local resonances-induced low-frequency band gaps in two-dimensional phononic crystal slabs with periodic stepped resonators *J. Phys. D: Appl. Phys.* **44** 055401
- [23] Xiao Y, Mace B R, Wen J and Wen X 2011 Formation and coupling of band gaps in a locally resonant elastic system comprising a string with attached resonators *Phys. Lett. A* **375** 1485–91
- [24] Xiao Y, Wen J and Wen X 2012 Flexural wave band gaps in locally resonant thin plates with periodically attached spring–mass resonators *J. Phys. D: Appl. Phys.* **45** 195401
- [25] Zhang H B, Chen J J and Han X 2012 Lamb wave band gaps in a homogenous plate with periodic tapered surface *J. Appl. Phys.* **112** 054503
- [26] Zhang S, Hui Wu J and Hu Z 2013 Low-frequency locally resonant band-gaps in phononic crystal plates with periodic spiral resonators *J. Appl. Phys.* **113** 163511
- [27] Yan X, Zhu R, Huang G L and Yuan F G 2013 Focusing flexural Lamb waves by designing elastic metamaterials bonded on a plate *Proc. SPIE* **8695** 86952P
- [28] Matlack K H, Bauhofer A, Krödel S, Palermo A and Daraio C 2016 Composite 3D-printed metastructures for low-frequency and broadband vibration absorption *Proc. Natl Acad. Sci.* **113** 8386–90
- [29] Li S, Chen T, Wang X, Li Y and Chen W 2016 Expansion of lower-frequency locally resonant band gaps using a double-sided stubbed composite phononic crystals plate with composite stubs *Phys. Lett. A* **380** 2167–72
- [30] Chen Y, Li T, Scarpa F and Wang L 2017 Lattice metamaterials with mechanically tunable Poisson's ratio for vibration control *Phys. Rev. Appl.* **7** 024012
- [31] Gao N, Wei Z, Hou H and Krushynska A O 2019 Design and experimental investigation of V-folded beams with acoustic black hole indentations *J. Acoust. Soc. Am.* **145** EL79–83
- [32] Li S, Dou Y, Chen T, Xu J, Li B and Zhang F 2019 Designing a broad locally-resonant bandgap in a phononic crystals *Phys. Lett. A* **383** 1371–7
- [33] Zhou G, Wu J H, Lu K, Tian X, Liang X, Huang W and Zhu K 2019 An approach to broaden the low-frequency bandwidth of sound insulation by regulating dynamic effective parameters of acoustic metamaterials *J. Phys. D: Appl. Phys.* **52** 215102

- [34] Liu C R, Wu J H, Lu K, Zhao Z T and Huang Z 2019 Acoustical siphon effect for reducing the thickness in membrane-type metamaterials with low-frequency broadband absorption *Appl. Acoust.* **148** 1–8
- [35] Ma F, Chen J and Wu J H 2019 Three-dimensional acoustic sub-diffraction focusing by coiled metamaterials with strong absorption *J. Mater. Chem. C* **7** 5131–8
- [36] Yu D, Liu Y, Zhao H, Wang G and Qiu J 2006 Flexural vibration band gaps in Euler–Bernoulli beams with locally resonant structures with two degrees of freedom *Phys. Rev. B* **73** 064301
- [37] Lu K, Wu J H, Jing L and Guan D 2017 Flexural vibration bandgaps in local resonance beam with a novel two-degree-of-freedom local resonance system *Eur. Phys. J. Appl. Phys.* **77** 20501
- [38] Huang G L and Sun C T 2010 Band gaps in a multiresonator acoustic metamaterial *J. Vib. Acoust.* **132** 031003
- [39] Tan K T, Huang H H and Sun C T 2012 Optimizing the band gap of effective mass negativity in acoustic metamaterials *Appl. Phys. Lett.* **101** 241902
- [40] Hussein M I and Frazier M J 2013 Metadamping: an emergent phenomenon in dissipative metamaterials *J. Sound Vib.* **332** 4767–74
- [41] Pai P F 2010 Metamaterial-based broadband elastic wave absorber *J. Intell. Mater. Syst. Struct.* **21** 517–28
- [42] Xiao Y, Wen J and Wen X 2012 Longitudinal wave band gaps in metamaterial-based elastic rods containing multi-degree-of-freedom resonators *New J. Phys.* **14** 033042
- [43] Pai P F and Peng H 2014 Acoustic metamaterial structures based on multi-frequency vibration absorbers *Proc. SPIE* **9064** 90641X
- [44] Pai P F, Peng H and Jiang S 2014 Acoustic metamaterial beams based on multi-frequency vibration absorbers *Int. J. Mech. Sci.* **79** 195–205
- [45] An X, Sun F, Yu P, Fan H, He S and Fang D 2015 Negative effective mass density of one-dimensional hierarchical metacomposite *J. Appl. Mech.* **82** 031002
- [46] Peng H and Pai P F 2015 Design of multi-stopband metamaterial plates for absorption of broadband elastic waves and vibration *Proc. SPIE* **9438** 94380X
- [47] Liu Y, Shen X, Su X and Sun C T 2016 Elastic metamaterials with low-frequency passbands based on lattice system with on-site potential *J. Vib. Acoust.* **138** 021011
- [48] Zhou X, Wang J, Wang R and Lin J 2016 Effects of relevant parameters on the bandgaps of acoustic metamaterials with multi-resonators *Appl. Phys. A* **122** 427
- [49] Lu K, Wu J H, Jing L, Gao N and Guan D 2017 The two-degree-of-freedom local resonance elastic metamaterial plate with broadband low-frequency bandgaps *J. Phys. D: Appl. Phys.* **50** 095104